ELSEVIER

Chemical Physics 265 (2001) 251–261

Chemical Physics

www.elsevier.nl/locate/chemphys

Computational study of the thermal reaction rate between $S^+(^4S)$ and acetylene

Massimiliano Aschi [a], Antonio Largo [b,*]

[a] *Dipartimento di Chimica, Universitá di Roma 'La Sapienza', P.le A. Moro 5, 00185 Rome, Italy*
[b] *Departamento de Química Fisica, Facultad de Ciencias, Universidad de Valladolid, 47005 Valladolid, Spain*

Received 23 October 2000

Abstract

The thermal reaction between $S^+(^4S)$ and acetylene has been studied in the framework of the statistical theories in order to extract informations concerning its actual efficiency at different temperatures and bath gas densities. The results of the present work are in reasonable agreement with the available experimental data concerning both the efficiency and the generated products. The spin-forbidden paths have been also re-addressed and their actual role within the overall process, discussed.

1. Introduction

In a recent paper [1], we have undertaken a theoretical ab initio study of the reaction of ground-state $S^+(^4S)$ with acetylene (1)

$$S^+(^4S) + C_2H_2 \rightarrow C_2HS^+(^3\Sigma) + H(^2S) \qquad (1)$$

which had previously received a great deal of attention [2–4] mainly due to its recognized role in the synthesis of interstellar C_2S. The main conclusions of the above work were: first, the reaction proceeds exothermically in agreement with previous experimental results; secondly, the reaction can in principle occur through two mechanisms, direct formation of the products on the quartet surface or, alternatively, along the doublet surface following spin inversion through intersystem crossing. In particular, the second mechanism was remarked as the only one which could realistically support the experimental observation [3] about the formation of a long-lived intermediate of general formula $SC_2H_2^+$.

In other words, reaction (1) was shown to formally provide a very interesting example of globally spin-allowed reaction occurring through spin-forbidden elementary steps. In our previous work only a preliminary evaluation of the probability for intersystem crossing employing the Landau–Zener approximation was carried out. Furthermore, since we did not perform a kinetic study, the actual role of spin inversion in the reaction could not be determined.

On the basis of the previous ab initio study, we decided to address the evaluation of the thermal rate coefficient for reaction (1) and its dependence on temperature and bath gas density, in the framework of the statistical kinetic theories [5]

* Corresponding author. Fax: +34-983-423-013.
E-mail address: alargo@qf.uva.es (A. Largo).

0301-0104/01/$ - see front matter
PII: S0301-0104(01)00242-7

whose critical application [6] has already demonstrated to furnish an efficient tool for investigating bimolecular reactions of relatively complex systems [7–20]. The results of this study, presented in this paper will allow a comparison with the experimental findings.

2. Previous theoretical findings

Our investigation is entirely based on the already mentioned G2(P) study [1] whose main features, on the basis of the potential energy diagram can be summarized as follows:

(1) The reaction commences on the quartet surface. The reactants approach each other on a $^4A_2$–$^4A''$ surface, progressing without adiabatic barriers to the complexes **3a** and **2a** (the relevant minima on the quartet and doublet $SC_2H_2^+$ surfaces are schematically represented in Fig. 1; (a) denotes species on the quartet surface, whereas (b) denotes minima on the doublet surface. A complete account of the geometrical parameters of the minima, as well as of the transition states connecting them, can be found in Ref. [1]). These latter structures, which are assumed to be in rapid conformational equilibrium, can directly evolve to the products through the **TS1a** structure by losing a hydrogen atom.

(2) Alternatively, provided an intersystem crossing has occurred during the encounter path, the reaction can proceed all along the $^2A''$ surface. In this case, three intermediates (**1b**, **4b** and **5b**), located on the doublet surface would be able both to lose a hydrogen atom giving rise to the products and also to mutually interconvert through the transition structures **TS2b** (**1b/4b**), **TS6b** (**1b/5b**). This second possibility was advanced because the intermediate **4b**, lying 110 kcal/mol below the reactant, fits the experimental findings reasonably well.

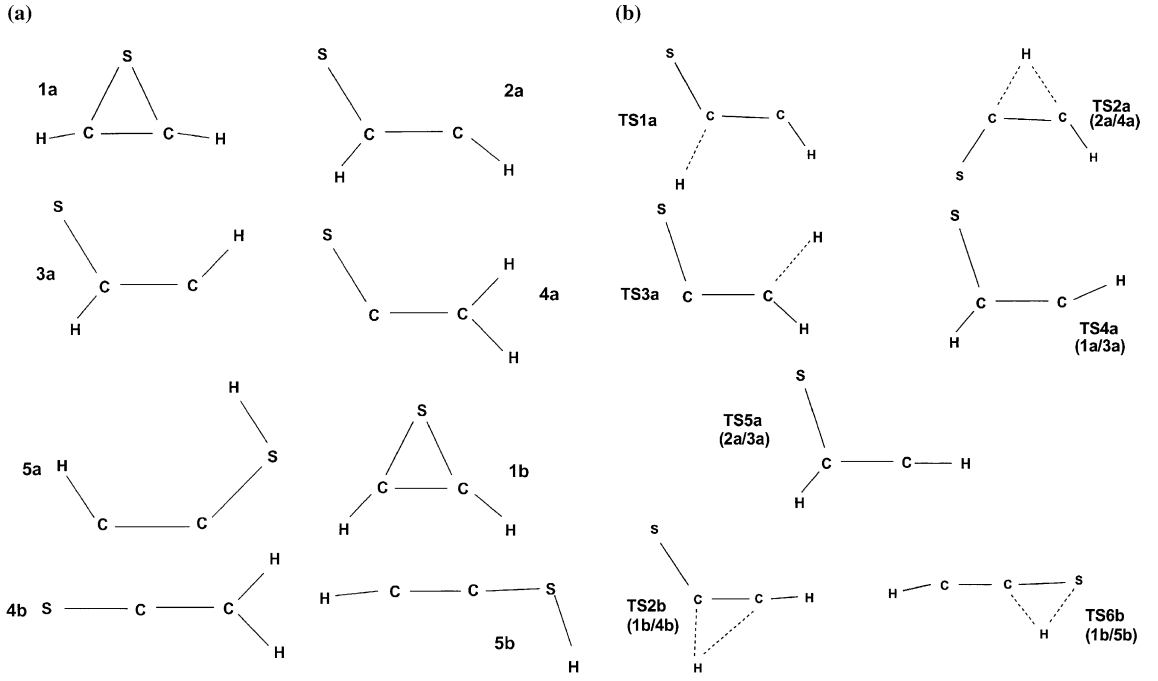

Fig. 1. Schematic representation of the more relevant minima and transition states on the $SC_2H_2^+$ (a) quartet and (b) doublet surfaces. The notation is the same employed in Ref. [1].

An important point for elucidating the mechanistic features of reaction (1), i.e. whether or not the evolution takes place on the doublet surface, is to assess where and to what extent the spin crossings actually occur. Our previous study was not explicitly devoted to the description of the spin-forbidden unimolecular chemistry of the system; however two crossing points were located on each of the two approaching paths, i.e. on the paths with C_{2v} and C_s symmetry, and were characterized both by a rather low energy barrier and by non-negligible spin-crossing probabilities as large as 0.015–0.048 and 0.063–0.187 respectively. However since they were actually described as taking place *after* the formation of the primary collision complex **1a**, the practically barrierless adiabatic evolution of the latter into **3a** and **2a**, obviously makes the lifetime of the latter and consequently [21,22] the probability of the spin crossing rather low at this stage of the reaction coordinate. Therefore the possibility of another, more competing spin-forbidden path involving **3a** and **2a** quartet calls for a preliminary reappraisal of the non-adiabatic chemistry of the system.

3. Reappraisal of the minimum energy crossing points

3.1. Computational details

As already shown in the literature [23], within the adiabatic representation two surfaces with different spin multiplicity can intersect each other in a space of dimension $F-1$ where F is the number of internal degrees of freedom. The minimum of the above hyperline, defined as the minimum energy crossing point (MECP), as pointed out by several authors [24], can be considered to play the role of the transition state in reactions taking place on a single surface. It is therefore of extreme importance to locate it on the Born–Oppenheimer surface. At this end several ab initio gradient-based methods have been developed in the past [25–28]. Recently we have proposed an extension of the above approaches which basically couples electronic energies and analytical gradients calculated at different levels of any theory [29]. In the present case two computational levels have been employed: an accurate optimization [29] was carried out employing density functional theory (DFT), in particular the B3LYP exchange-correlation functional [30] with the 6-311+G(d) basis set [31], and subsequently refined at the CCSD(T)/cc-pVTZ//B3LYP/6-311+G(d), where the latter notation denotes coupled cluster [32] energies in conjunction with B3LYP analytical gradients (in the CCSD(T) calculations the correlated consistent cc-pVTZ basis set of Dunning [33,34] was employed). An estimation of the curvature of the seam [28,29] and therefore a crude determination of the zero point vibrational energy at the MECPs has also been carried out. Spin–orbit coupling matrix elements between all the doublet and quartet substates, which give an estimation of the magnitude of the coupling between the two surfaces, have been calculated for the MECPs structures using first-order configuration interaction (FOCI) wavefunctions constructed with the cc-pVTZ basis set and with an approximate monoelectronic [35] hamiltonian. All these calculations have been carried out using the GAUSSIAN 94 [36] and GAMESS USA [37] packages. To ascertain the actual role played by the located MECPs, i.e. which minima are actually interconnected through MECPs, a rough IRC-like procedure has been applied [38].

3.2. Results

Two structures, **MECP1** and **MECP2**, have been located along the $(F-1)$-dimensional hyperline of doublet–quartet intersection and characterized as minima along that seam. They are shown in Fig. 2 and formally correspond to the unimolecular interconversion of **3a** to **1b** and **2a** to **4b** respectively. The first of these structures was located just 3 kcal/mol above **3a**, whereas the second one was found about 27 kcal/mol above **2a**. It should be remarked however, that the analysis of the coordinate orthogonal to the seam, i.e. associated to the spin crossover in the second channel (that implying interconversion from **2a** to **4b**),

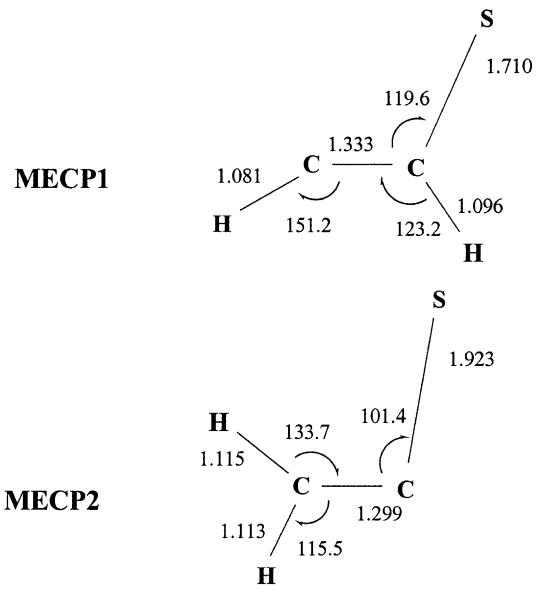

Fig. 2. B3LYP/6-311+G(d) geometries of the minimum energy crossing points, **MECP1** and **MECP2**. Distances are given in Å and angles in degrees.

formally reveals the involvement of the hydrogen atom motion, and so the tunnel effect probably plays in this case a more pronounced role [39]. Both of these MECPs, show a relatively large value of spin–orbit coupling matrix element of 99 and 101 cm^{-1} respectively.

4. Mechanistic model

On the basis of the above findings, and combined with the results of our previous study [1], we can outline the following mechanistic pattern which will be the basis of the kinetic study reported in the following:

- The formation of the **3a/2a** complex takes place directly along the initial path; in other words, the competition between adiabatic (**TS4a**) and non-adiabatic (crossing to **1b**) is considered completely unbalanced toward the former.
- The intersystem crossing will take place much more efficiently from **3a/2a** leading to the doublet intermediates **1b** and **4b**. However, a competition of the adiabatic channel through **TS1a** cannot a priori be ruled out as will be shown below.

In conclusion, our overall reaction appears in Scheme 1.

5. Kinetic calculations

5.1. Details

According to the picture depicted in Scheme 1 we have followed the general criteria of treating the formation of the initial intermediate **3a/2a** in

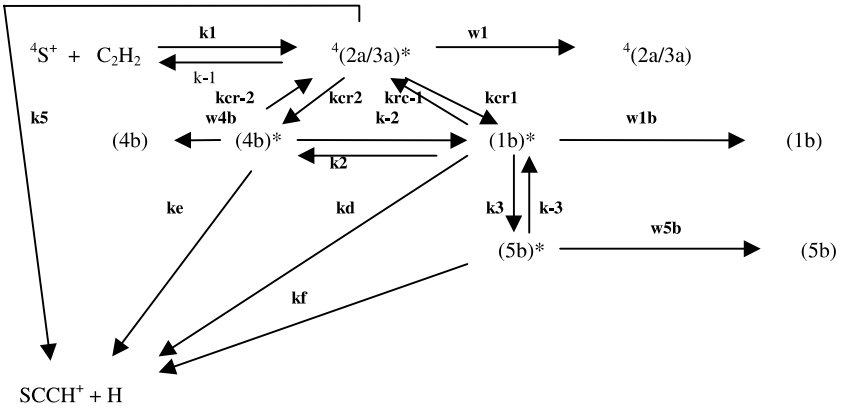

Scheme 1. Mechanistic model for the kinetic study employed in the present work.

terms of the microcanonical variational transition state theory (μVTST) in its vibrator formulation [1] [40,41]

$$k_{\text{capture}}(E,J) = W_i^{\mu\text{VTS}}(E,J)/[hQ_r(T)], \tag{2}$$

where $W_i^{\mu\text{VTS}}(E,J)$ is the sum of the states calculated variationally along the collision path (see below) and $Q_r(T)$ is the reactants [2] partition function excluding the motion of the centre of mass and assuming the electronic contribution as equal to 4, i.e. neglecting the temperature effect. The subsequent unimolecular evolution of the same complex was treated in terms of multichannel RRKM theory. At this end the microcanonical rate coefficients were calculated in correspondence of all the intermediates for values of E starting from the entrance channel at different J. Such unimolecular rate coefficients have been calculated for each ith channel according to the usual formula [42]:

$$k_i(E,J) = \int \kappa(E,J)\rho_i^{\#}(E-E^{\#},J)\mathrm{d}E/[h\rho_i(E,J)], \tag{3}$$

where $\rho^{\#}(E-E^{\#},J)$ is the density of the states for the transition structure related to the process ith, $\rho_i(E,J)$ is the density of the states of the starting dissociating intermediate, h is the Planck constant and $\kappa(E,J)$ is the monodimensional tunnelling probability according to the generalized Eckart potential [43]. The determination of the $\rho^{\#}(E-E^{\#},J)$ term has been calculated through Forst's algorithm [44] using the corresponding frequencies and moments of inertia depending on the nature of the transition state (TS). For tight TSs, i.e. corresponding to first-order saddle points on the Born–Oppenheimer hypersurface, the calculated real frequencies and moments of inertia have been employed. For loose TSs, i.e. barrierless capture and dissociations as already stated, we have adopted the μVTST. At this end, we have followed the reaction coordinate corresponding to the loss of S^+ from the quartet **3a** structure, corresponding to the reactants capture path, and the loss of H from the **4b**, **5b**, **1b** doublet intermediates with steps of 0.1 A at the QCISD(T)/6-311G*/MP2(full)/6-31G* level of theory (QCISD(T) means quadratic configuration interaction including single and doubles substitutions and a perturbative treatment of triple substitutions; MP2 stands for second-order Moller–Plesset perturbation theory). At each step the MP2(full)/6-31G* hessian has been calculated and then corrected by projecting out the centre of mass translation and external rotations, as well as the reaction coordinate using the standard Miller algorithm, obtaining the $3N-7$ modes orthogonal to the path [45]. With these parameters, the sum of the states was minimized for every E and J value obtaining the loose-TS locations. For the unimolecular spin-forbidden reactions we have described the rate coefficient using a non-adiabatic (n.a.) version of the RRKM theory [46–48]:

$$k_i^{\text{n.a.}}(E,J) = (2/h)\int \mathrm{d}E_h p(E_h,J)\rho_i^{\text{MECP}} \times (E-E_h,J)/\rho_i(E,J), \tag{4}$$

where E_h is the fraction of the non-fixed energy reversed in the coordinate orthogonal to the seam, $p(E_h,J)$ is the surface hopping probability which has been calculated according to the monodimensional Delos formula

$$p(E) = 4\pi^2 V^2 (2\mu/h^2 F\Delta F)^{2/3}\mathrm{Ai}^2(E(2\mu\Delta F^2/h^2F^4)^{1/3}), \tag{5}$$

where V is the doublet–quartet spin–orbit coupling matrix element at the MECP, μ is the reduced mass along the direction orthogonal to the seam, ΔF and F are respectively the norm of the difference of the gradients and their geometric mean; finally Ai is the Airy function. The latter approach is generally more suitable for weak-coupling surfaces and, unlike the Landau–Zener approach, is active also *below* the crossing point [49,50]; $\rho_i^{\text{MECP}}(E-E_h,J)$ is the density of the states at the crossing point which was calculated according to

[1] Of course the assumption of the non separability in the treatment of conserved and transitional modes along the path could induce a certain degree of error which however in this case, as described later did not result so severe.

[2] The reactants are assumed to be initially in thermal equilibrium.

the above cited Forst procedure using the corresponding harmonic frequencies calculated according to standard procedures (see above).

The w_i terms, i.e. the effective collision frequencies, were calculated using the standard equation

$$w = \beta c Z_{LJ}[M] \tag{6}$$

where βc is determined through Troe's weak-collision model [51] and Z_{LJ} and $[M]$ are the Lennard-Jones collision frequency and the bath gas (He) density.

The calculations have been performed at temperatures of the reagents ranging from 100 to 1000 K and at bath gas concentrations from 0 to 0.046 $\mathrm{mol\,l^{-1}}$. The steady-state solution of the master equation related to the Scheme 1 leads to the following microcanonical expression of the overall rate coefficient:

$$k_{(C_2HS^+)} = k_1/(LH)(k_eF/Ek_dG + k_fk_3/C + k_5), \tag{7}$$

$$k_{(C_2H_2S^+)} = w_{4b}(F/E)k_1/(LH) + w_{1b}Gk_1/(LH) + w_{5b}k_1k_3/CGk_1/(LH), \tag{8}$$

and

$$k_{overall} = k_{(C_2HS^+)} + k_{(C_2H_2S^+)}, \tag{9}$$

where

$$L = 1 - k_{cr-2}F/(HE) - k_{cr-1}G/H, \tag{10}$$

$$H = k_{-1} + w1 + k_{cr2} + k_{cr1} + k_5, \tag{11}$$

$$F = k_{cr2}/A + k_2k_{cr1}/(ABD), \tag{12}$$

$$G = k_{cr1}/(BD) + k_{-2}F/(BDE), \tag{13}$$

$$E = 1 - k_2k_{-2}/(ABD), \tag{14}$$

$$D = 1 - k_3k_{-3}/(BC), \tag{15}$$

$$A = k_{cr-2} + k_{-2} + k_e + w_{4b}, \tag{16}$$

$$B = k_3 + k_2 + k_d + k_{cr-1} + w_{1b}, \tag{17}$$

$$C = k_f + k_{-3} + w_{5b}. \tag{18}$$

The above expression were finally thermal averaged obtaining the final expressions:

$$k_{(C_2HS^+)}(T) = (1/hQ_r(T))\sum(2J+1) \times \int dE[W_i^{mVTS}(E,J)/(LH) \times (k_eF/Ek_dG + k_fk_3/C + k_5)]\exp(-E/kT), \tag{19}$$

$$k_{(C_2H_2S^+)}(T) = (1/hQ_r(T))\sum(2J+1) \times \int dE[W_i^{mVTS}(E,J)] \times [w_{4b}(F/E)/(LH) + w_{1b}G/(LH) + w_{5b}k_1k_3/CG/(LH)]\exp(-E/kT). \tag{20}$$

5.2. Results

The harmonic frequencies and rotational constants of the involved species are collected in Tables 1 and 2. The results of the above calculations are summarized in Fig. 3.

5.2.1. Temperature effect on the overall reaction

A not surprising negative temperature effect is observed both at low and large bath gas pressures, as can be seen in Fig. 3. Such result could be realistically explained by the fact that, as already shown in the previous paper, the title reaction is actually a barrier-free process whose reactive bottleneck can be ascribed just to an angular-momentum-conservation effect giving rise to the observed anti-Arrhenius behaviour.

Worth of remark is also the satisfactory agreement between our results and the available experimental data collected in thermal conditions. The absolute values of the experimental rate constants of 9.5×10^{-10} $\mathrm{s^{-1}\,cm^3\,molec^{-1}}$ from Smith et al. SIFT study [2] and the 9.8×10^{-10} $\mathrm{s^{-1}\,cm^3\,molec^{-1}}$ from Anicich and Huntress FT-ICR experiments [4], are both in reasonable agreement with our values at 300 K ranging between 1.2×10^{-9} and 1.57×10^{-9}.

Table 1
Vibrational frequencies (cm^{-1}) and rotational constants (GHz) for the different minima on the quartet and doublet $(SC_2H_2)^+$ surfaces (the notation of the species is the same as in Ref. [1])

	1a	2a	3a	4a	1b	4b	5b
Vibrational	238	425	362	284	728	341	271
frequencies	511	651	687	476	733	347	315
	528	808	750	723	791	857	706
	748	960	787	932	988	879	709
	810	982	789	955	1005	931	791
	913	1295	1159	1319	1418	1352	968
	1929	1384	1401	1465	1554	1608	2026
	3368	3085	3004	3030	3324	3090	2540
	3463	3290	3239	3141	3337	3204	3375
A	34.4	72.4	63.9	91.2	32.4	284.6	282.9
B	4.6	6.7	6.6	6.1	12.4	5.7	5.7
C	4.1	6.1	6.0	5.7	9.0	5.6	5.6

Table 2
Vibrational frequencies (cm^{-1}) and rotational constants (GHz) for the different TS on the quartet and doublet $(SC_2H_2)^+$ surfaces, as well as of the minimum energy crossing points (the notation of the species is the same as in Ref. [1])

	TS1a	TS2a	TS3a	TS4a	TS5a	TS2b	TS6b	MECP1	MECP2
Vibrational	627i	1577i	1376i	429i	606i	572i	1001i		
frequencies	358	245	174	298	393	589	306	185	455
	380	372	360	719	649	596	323	226	570
	484	708	538	787	723	644	642	681	777
	555	743	633	937	759	829	694	766	787
	619	862	828	1007	1151	1046	731	949	1131
	878	1436	911	1995	1419	1672	1837	1235	1331
	1715	2188	1794	3346	2959	2833	2182	2737	2974
	3334	3147	3264	3491	3336	3278	3352	2856	3186
A	93.0	81.7	122.2	52.0	69.5	90.8	367.9	51.0	55.0
B	6.1	6.3	5.8	5.4	6.5	6.0	5.6	6.8	7.0
C	5.7	5.9	5.5	4.9	6.0	5.6	5.5	6.1	6.2

5.2.2. Effect of the bath gas density on the overall reaction

In Fig. 4 we have reported the calculated efficiency versus the bath gas density at different temperatures. The available experimental data collected at thermal conditions, i.e. the FT-ICR [4] and SIFT [2] results, are marked with a circle. Again, it is evident the above remarked negative temperature dependence of the reaction efficiency as well as the satisfactory agreement with the experiment. Moreover, the bath gas density seems to increase the overall reaction efficiency. Such effect, not unexpected if one considers that the larger is the bath gas density less competitive will be the back dissociation is also in substantial agreement with the experimental observation of Zakouril et al. [3].

It is interesting to observe that such effect appears as ''temperature dependent''. The reaction occurring at higher temperatures seems to be less sensitive to the bath gas. This finding can be rationalized on the basis of the drastic decrease of the lifetime of the primary encounter complex at larger relative kinetic energies and/or temperatures.

Similarly, at temperatures of about 100 K, the pressure effect seems to slightly decrease respect to its effect at 300 K. Such trend, even though within

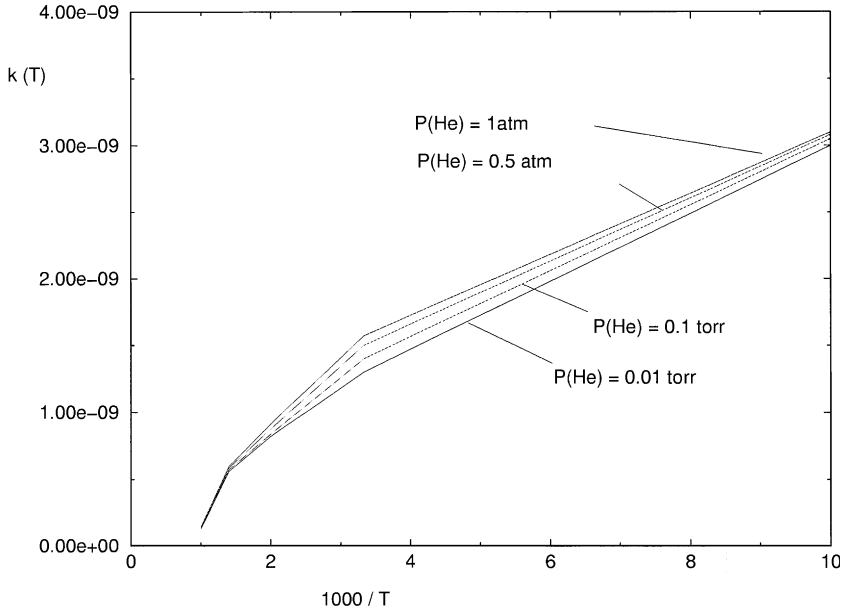

Fig. 3. Overall thermal rate coefficients ($cm^3 s^{-1} molec^{-1}$) plotted versus temperature (K) at different bath gas densities. The indicated pressures refer to 300 K.

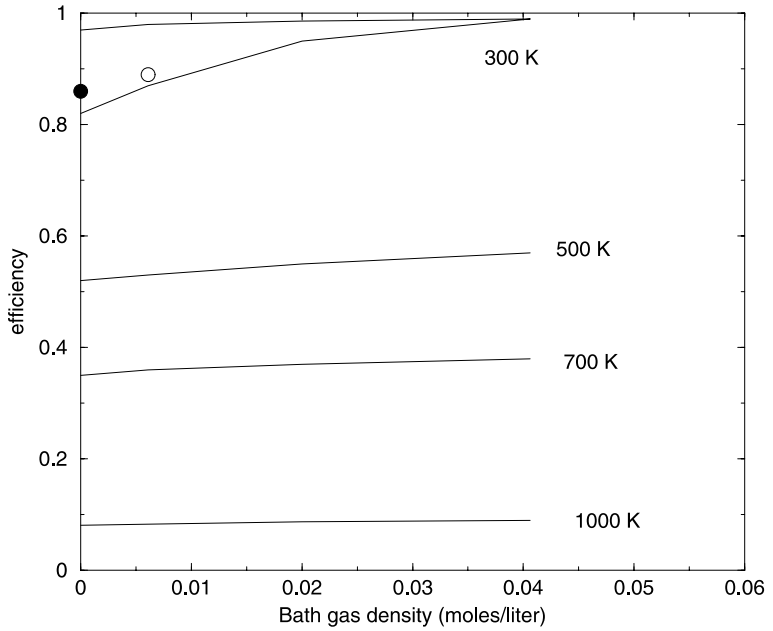

Fig. 4. Reaction efficiency plotted at different temperatures, versus the bath gas densities. Full and open circles refer to FT-ICR and SIFT experiments respectively.

the accuracy of the method, probably reflects the fact that the lower is temperature the colder is the primary formed species and less important is the bath gas quenching on the reaction efficiency.

Again, such observation is consistent with the experiment of Zakouril et al. [3], where the pressure dependence was found to be negatively dependent of the kinetic energy at the centre of mass of the reactants.

5.2.3. Branching ratios

In Table 3 we report the products molar ratios of reaction (1) at different temperatures and bath gas densities. It is readily seen that the channel leading to $C_2HS^+ + H$ is by far the most efficient one, as expected from simple thermodynamic arguments and as experimentally found in SIFT, SIFDT and FT-ICR. However our study shows that at every temperature value there is a non-negligible amount of secondary products which are formed mainly by **4b**, and to a lesser extent also by **1b** and **5b**. This finding is in disagreement with the results of Smith et al., where a 100% of C_2HS^+/H product was reported, but on the other hand it fits the more recent paper by Zakouril et al. in SIFDT conditions, where a secondary long-lived intermediate (presumably of connectivity **4b**) was invariably observed in the drift tube experiment. However, we wish here to underline that in the above paper the percentage of intermediate was a bit larger (≈20%) than in the present case. This slight discrepancy, whose absolute value is however unimportant if one considers both the experimental and the computational errors, reflects both the differences in the drift experiment and in the present calculations, and probably also the poorer quenching ability of Helium rather than the experimentally employed bath gas containing a certain amount of molecular nitrogen.

5.2.4. Outline of the mechanistic features

As introduced in the above section, one of the key points of the mechanism is the actual competition between the adiabatic path **a**, i.e. through **TS1a**, and the spin-forbidden channel, i.e. through **MECP1** and **MECP2**, conceivably taking place from the nascent **2a/3a** species. In Fig. 5 we have compared the values of the corresponding rate coefficients calculated at $J = 0$ condition spanning a large range of internal energy of the starting intermediate. It can be seen in Fig. 5 that at the energy values which are of a certain interest for the present thermal reaction, the non-adiabatic path is by far the most efficient one. This is not surprising at all. In fact, as already shown in the description of the PES, both MECPs lie much lower in energy than the **TS1a** structure. As a consequence of this finding, even though the large amount of internal energy reversed in the coordinate orthogonal to the seam actually decreases the hopping probability as shown in the probability equation (5), the consequently huge number of seam-crossings increases the global rate coefficient. However at high internal energy values, i.e. at very high collision energies, the adiabatic path **a** becomes more

Table 3
Products molar ratios for reaction (1), reported at three different temperatures (K) and bath-gas (He) densities (mol dm^{-3})

Temperature	He density	$C_2HS^+ + H$	**4b**	**5b**	**1b**
100	0.81×10^{-5}	0.973	0.023	0.003	0.001
	0.0061	0.971	0.025	0.003	0.001
	0.020	0.967	0.030	0.002	0.001
	0.0496	0.958	0.037	0.003	0.002
300	0.81×10^{-5}	0.971	0.025	0.003	0.001
	0.0061	0.970	0.026	0.003	0.001
	0.020	0.965	0.032	0.002	0.001
	0.0496	0.957	0.038	0.003	0.002
1000	0.81×10^{-5}	0.972	0.024	0.003	0.001
	0.0061	0.970	0.026	0.003	0.001
	0.020	0.968	0.029	0.002	0.001
	0.0496	0.958	0.037	0.003	0.002

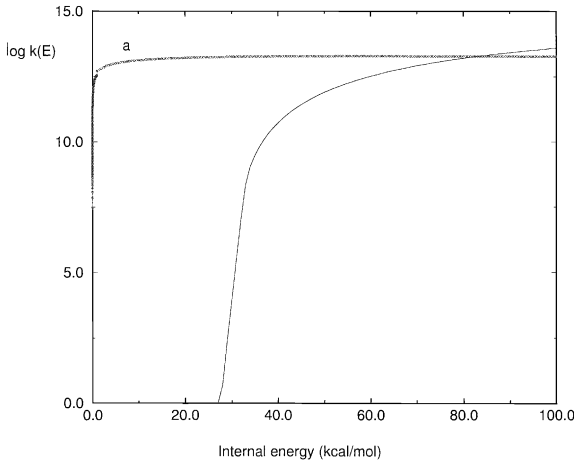

Fig. 5. $J = 0$ microcanonical rate coefficients ($cm^3\,s^{-1}\,molec^{-1}$), for the competing (see text) non-adiabatic (curve a) and adiabatic unimolecular chemistry of **2a/3a**.

competitive giving rise to the characteristic curvature for the non-adiabatic coefficient. It should however be pointed out that at higher internal energies both the statistical and the harmonic approximations become much weaker and a more specifically dynamic approach would be required.

However it can be definitely established that, at least for the thermal regime we were interested at, the path taking place directly on the quartet surface is hardly likely to occur.

6. Conclusions

The present study conducted at different temperature and pressure regimes shows that reaction (1) is a highly efficient reaction basically at every explored condition. This conclusion is not surprising in the light of the previous theoretical findings and is in agreement with the available experimental results from different laboratories. This result confirms that the reaction of S^+ ions with acetylene might play a crucial role in the synthesis of C_2S in the interstellar medium.

A reasonable agreement is observed between our computed rate coefficient (in the range $(1.2–1.57) \times 10^{-9}$ $s^{-1}\,cm^3\,molec^{-1}$) and the results from different experiments (9.5×10^{-10} and 9.8×10^{-10} $s^{-1}\,cm^3\,molec^{-1}$). Perhaps the major sources of error in our calculations are the possibility of non-RRKM behaviour of the **2a/3a** multichannel evolution, as well as the intrinsic limitations of the monodimensional treatment of spin crossing processes.

A negative temperature effect has been observed, which is not surprising for a barrier-free process occurring almost at collisional efficiency as observed in the experiments. The bath gas density has only a relatively small effect on the rate coefficient, and its influence has an interesting temperature dependence.

Concerning the branching ratios our calculations agree with the experimental results in that the channel leading to C_2HS^+/H is by far the most efficient one. However a non-negligible amount of secondary products is observed at all temperatures in the presence of a quencher bath gas. The dominant secondary species, **4b**, agrees well with the intermediate observed in the SIFDT experiments of Zakouril et al.

Another interesting point is the role of spin-crossover in reaction (1). According to our calculations, at low energies spin-crossover prevails over the adiabatic path, a tendency which is reversed at high collisional energies. Therefore the main conclusion of our work is that at thermal regime spin crossover should be the most competitive path for the reaction of S^+ with acetylene. From a more global perspective this reaction exemplifies the importance that spin-forbidden steps may play even in spin-allowed reactions. In this particular case only the introduction of spin-crossover explains the main experimental features observed for this reaction.

Acknowledgements

M.A. would like to thank Prof. Alfredo Di Nola (University of Rome) for a grant and Dr. Jeremy N. Harvey (University of Bristol) for several helpful discussions. A.L. wishes to thank financial support from the Ministerio de Educacion y Cultura of Spain (DGICYT, Grant PB97-0399-C03-01) and by the Junta de Castilla y Leon (Grant VA 18/00B).

References

[1] C. Barrientos, P. Redondo, A. Largo, Chem. Phys. Lett. 306 (1999) 168.
[2] D. Smith, N.G. Adams, K. Giles, E. Herbst, Astron. Astrophys. 200 (1988) 191.
[3] P. Zakouril, J. Glosik, V. Skalsky, W. Lindinger, J. Phys. Chem. 99 (1995) 15890.
[4] V.G. Anicich, W.T. Huntress, Astrophys. J. 62 (1986) 553.
[5] D.G. Truhlar, B.C. Garret, S.J. Klippenstein, J. Phys. Chem. 100 (1996) 12771.
[6] J. Espinosa-Garcia, F.J. Olivares, J.C. Corchado, Chem. Phys. 183 (1994) 95.
[7] J. Troe, in: M. Baer, C.-Y. Ng, Advance in Chemical Physics, vol. LXXXII, Wiley, New York, 1992, p. 485.
[8] R.G. Gilbert, S.C. Smith, Theory of Unimolecular and Recombination Reactions, Blackwell Scientific, Oxford, 1990.
[9] J.I. Steinfield, J.S. Francisco, W.L. Hase, Chemical Kinetics and Dynamics, Prentice Hall, Englewood Cliffs, 1989.
[10] D.G. Thrular, A.D. Isaacson, B.C. Garret, in: M. Baer (Ed.), The Theory of Chemical Reactions, vol. 4, Chemical Rubber, Boca Raton, FL, 1985.
[11] W. Chesnavich, M.T. Bowers, in: M.T. Bowers (Ed.), Gas Phase Ion Chemistry, vol. 1, Academic Press, New York, 1979, p. 119.
[12] B.D. Wladkowski, K.F. Lim, W.D. Allen, J.I. Brauman, J. Am. Chem. Soc. 114 (1992) 9136.
[13] W.-C. Diau, S.C. Smith, J. Phys. Chem. 100 (1996) 12349.
[14] H. Wang, W.L. Hase, J. Am. Chem. Soc. 119 (1997) 3039.
[15] J.B. Lipson, T.W. Beiderhase, L.T. Molina, M.J. Molina, M. Olzmann, J. Phys. Chem. A 103 (1999) 6540.
[16] Z.-F. Xu, S.-M. Li, Y.-X. Yu, Z.-S. Li, C.-C. Sun, J. Phys. Chem. A 103 (1999) 4910.
[17] H. Hou, B. Wang, Y. Gu, J. Phys. Chem. A 104 (2000) 320.
[18] J. Espinosa-Garcia, J. Phys. Chem. A 104 (2000) 7537.
[19] J.A. Miller, S.J. Klippenstein, S.H. Robertson, J. Phys. Chem. A 104 (2000) 7525.
[20] J. Villa, J.C. Corchado, A. Gonzalez-Lafont, J.M. Lluch, D.G. Thrular, J. Phys. Chem. A 103 (1999) 5061.
[21] J.C. Tully, J. Chem. Phys. 61 (1974) 61.
[22] G.E. Zahr, R.K. Preston, W.H. Miller, J. Chem. Phys. 62 (1975) 1127.
[23] L. Salem, Electrons in Chemical Reactions, Wiley, New York, 1982.
[24] J.C. Lorquet, in: T. Baer, C.Y. Ng, I. Powis (Eds.), The Structure, Energetics and Dynamics of Organic Ions, Wiley, New York, 1996.
[25] D.R. Yarkony, in: D.R. Yarkony (Ed.), Modern Electronic Structure Theory, World Scientific, Singapore, 1995.
[26] M.J. Bearpark, M.A. Robb, H.B. Schlegel, Chem. Phys. Lett. 223 (1994) 269.
[27] A. Faradzel, M. Dupuis, J. Comput. Chem. 12 (1991) 276.
[28] N. Koga, K. Morokuma, Chem. Phys. Lett. 119 (1985) 371.
[29] J.N. Harvey, M. Aschi, H. Schwarz, W. Koch Theor, Chem. Acc. 99 (1998) 95.
[30] A.D. Becke, J. Chem. Phys. 98 (1993) 5648.
[31] R. Krishnan, J.S. Binkley, R. Seeger, J.A. Pople, J. Chem. Phys. 72 (1980) 650.
[32] K. Raghavachari, G.W. Trucks, J.A. Pople, M. Head-Gordon, Chem. Phys. Lett. 157 (1989) 479.
[33] T.H. Dunning, J. Chem. Phys. 90 (1989) 1007.
[34] D.E. Woon, T.H. Dunning, J. Chem. Phys. 98 (1993) 1358.
[35] S. Koseki, M.W. Schmidt, M.S. Gordon, J. Phys. Chem. 96 (1992) 10768.
[36] M.J. Frisch, G.W. Trucks, H.B. Schlegel, P.M.W. Gill, B.G. Johnson, M.A. Robb, J.R. Cheeseman, T. Keith, G.A. Petersson, J.A. Montgomery, K. Raghavachari, L.A. Al-Laham, V.G. Zakrzewski, J.V. Ortiz, J.B. Foresman, J. Cioslowski, B.B. Stefanov, A. Nanayakkara, M. Challacombe, C.Y. Peng, P.Y. Ayala, W. Chen, M.W. Wong, J.L. Andres, E.S. Replogle, R. Gomperts, R.L. Martin, D.J. Fox, J.S. Binkley, D.J. Defrees, J. Baker, J.P. Stewart, M. Head-Gordon, C. Gonzalez, J.A. Pople, GAUSSIAN 94, revision D.1, Gaussian Inc., Pittsburgh, PA, 1995.
[37] M.W. Schmidt, K.K. Baldridge, J.A. Boatz, S.T. Elbert, M.S. Gordon, J.H. Hensen, S. Koseki, N. Matsunaga, K.A. Nguyen, S.J. Su, T.L. Windus, M. Dupuis, J.A. Montgomery, J. Comput. Chem. 14 (1992) 1910.
[38] D. Schroeder, C. Heinemann, H. Schwarz, J.N. Harvey, S. Dua, S.J. Blanskby, J. Bowie, Chem. Eur. J. 4 (1998) 2550.
[39] J.N. Harvey, S. Grimme, M. Woeller, S.D. Peyerimhoff, D. Danovich, S. Shaik, Chem. Phys. Lett. 322 (2000) 358.
[40] B.C. Garrett, D.G. Truhlar, J. Chem. Phys. 70 (1979) 1593.
[41] X. Hu, W.L. Hase, J. Chem. Phys. 95 (1991) 8073.
[42] P.J. Robinson, K.A. Holbrook, Unimolecular Reactions, Wiley, New York, 1972.
[43] W.H. Miller, J. Am. Chem. Soc. 101 (1979) 6810.
[44] W. Forst, Theory of Unimolecular Reactions, Academic Press, New York, 1973.
[45] W.H. Miller, N.C. Handy, J.E. Adams, J. Chem. Phys. 72 (1980) 99.
[46] J.C. Lorquet, B. Leyh-Nihant, J. Phys. Chem. 92 (1988) 4778.
[47] K. Morokuma, Q. Cui, Z. Liu, Faraday Discuss. 110 (1998) 71.
[48] M. Aschi, J.N. Harvey, Phys. Chem. Chem. Phys. 1 (1999) 5555.
[49] J.B. Delos, W.R. Thorson, Phys. Rev. A 6 (1972) 728.
[50] J.B. Delos, J. Chem. Phys. 59 (1973) 2365.
[51] J. Troe, J. Phys. Chem. 83 (1979) 114.